Hyperfine Interact (2019) 240: 94
https://doi.org/10.1007/s10751-019-1618-3

Combined analysis of the low-energy enhancement of the gamma-strength function and the giant dipole resonance

Cebo Ngwetsheni[1] · **José Nicolás Orce**[1]

Published online: 20 August 2019

Abstract
The nuclear dipole polarizability is mainly governed by the dynamics of the giant dipole resonance and has been investigated along with the effects of the low-energy enhancement of the photon strength function for nuclides in medium- and heavy-mass nuclei. Cubic-spline interpolations to both data sets show a significant reduction of the nuclear dipole polarizability for semi-magic and doubly magic nuclei, with magic numbers $N = 28$, 50, 82 and 126, which supports shell effects at high-excitation energies from the quasi-continuum to the giant dipole resonance. This work expands on the data analysis of our recent publication in Ngwetsheni and Orce (Phys. Lett. B **792**, 335, 2019), which reveals a new spectroscopic probe to search for "old" and "new" magic numbers at high-excitation energies. New results presented in this work suggest an even higher sensitivity of the nuclear polarizability to shell effects when extrapolating the low-energy enhancement at lower gamma-ray energies.

Keywords Nuclear dipole polarizability · Quasi-continuum · Low-energy enhancement · Photon-strength function · Photo-absorption cross sections · Shell model · Magic numbers

1 Introduction

Matter in the vicinity of an electromagnetic (EM) field tends to polarize as a result of a perturbation of the charge distribution. In the case of the nucleus, the polarizability is dominated

This article is part of the Topical Collection on *Proceedings of the International Conference on Hyperfine Interactions and their Applications (HYPERFINE 2019), Goa, India, 10-15 February 2019* Edited by S. N. Mishra, P. L. Paulose and R. Palit

This work was supported by the National Research Foundation of South Africa, the MaNus/MatSci program and the SA-CERN collaboration.

✉ Cebo Ngwetsheni
3344489@myuwc.ac.za

✉ José Nicolás Orce
jnorce@uwc.ac.za

[1] Department of Physics & Astronomy, University of the Western Cape, P/B X17, Bellville, ZA-7535, South Africa

by the dynamics of the isovector giant dipole resonance (GDR) [1, 2], which is observed as a wide peak – with a full width at half-maximum of about 4-5 MeV for closed-shell nuclei, which becomes broader as nuclei deform – in photo-absorption cross-section measurements. The GDR is a collective motion that can be initiated by reactions which favor $\Delta L = 1$ and $\Delta T = 1$, e.g. gamma absorption (real photons) or Coulomb excitation (virtual photons). The GDR is described macroscopically according to the liquid drop model as the inter-penetrating motion of proton and neutron fluids out of phase, resulting from the nuclear symmetry energy a_{sym} in the Bethe-Weizsäcker semi-empirical mass formula [3, 4] acting as a restoring force [1],

$$a_{sym}(\rho_N - \rho_Z)^2/\rho_A, \tag{1}$$

where ρ_N, ρ_Z and ρ_A are the neutron, proton and total mass densities, respectively. Using the liquid drop model, with potential energy ρ_Z, Migdal calculated the ground state (g.s.) electric dipole polarizability $\alpha_{E1} = \frac{\mathbf{P}}{\mathbf{E}}$, where $\mathbf{P}$ is the electric dipole moment and $\mathbf{E}$ the electric field strength, connecting to a_{sym} as follows,

$$\alpha_{E1} = \frac{e^2 R^2 A}{40 a_{sym}} = 2.25 \times 10^{-3} A^{5/3}\ \text{fm}^3, \tag{2}$$

where $a_{sym} = 23$ MeV was assumed by Migdal as well as a defined spherical surface of radius $R = 1.2A^{1/3}$ fm [1]. Hence, α_{E1} is proportional to the size and diffuseness of the nucleus. As a second-order effect in perturbation theory, α_{E1} is also related to the total photo-absorption cross section σ_{total} and its (-2) moment, σ_{-2}, in the following manner [5],

$$\alpha_{E1} = 2e^2 \sum_n \frac{\langle i \parallel \hat{E1} \parallel n\rangle\langle n \parallel \hat{E1} \parallel i\rangle}{E_\gamma} = \frac{\hbar c}{2\pi^2}\sigma_{-2}, \tag{3}$$

where $\hat{E1}$ is the electric dipole operator, $|i\rangle$ and $|n\rangle$ are the ground and excited state vectors and σ_{-2} is defined as,

$$\sigma_{-2} := \int_0^{E_{\gamma max}} \frac{\sigma_{total}(E_\gamma)}{E_\gamma^2}\, dE_\gamma, \tag{4}$$

where $E_{\gamma_{max}}$ is dependent on experiment (e.g., photo-neutron cross sections are measured above neutron threshold [6]). Additionally, a new empirical formula for σ_{-2} [7] has been determined from the 1988 photoneutron cross-section evaluation using monoenergetic photons [6],

$$\sigma_{-2} = 2.4\kappa\ A^{5/3}\mu\text{b/MeV}, \tag{5}$$

where the polarizability parameter κ is included to account for deviations from the actual GDR effects to that predicted by the hydrodynamic model [1, 8]. The polarizability parameter κ can therefore be extracted for known σ_{-2} values and vice versa.

The sum rule in Eq. 3 indicates that large $E1$ matrix elements via virtual excitations of the *GDR* [9] may polarize the shape of the ground state $|i\rangle$. Similarly, two-step processes of the type $|i\rangle \rightarrow |n\rangle \rightarrow |f\rangle$ (e.g. $0_1^+ \rightarrow 1^-_{GDR} \rightarrow 2_1^+$) can polarize the shape of final excited states $|f\rangle$. This polarization phenomenon is the so-called $E1$ *polarizability* – which is directly related to α – and may compete with the reorientation effect, RE; both being second-order effects in Coulomb-excitation theory [10–13]. The RE generates a time-dependent hyperfine splitting of nuclear levels which depend on their shape, and can be used to determine spectroscopic quadrupole moments or Q_s values [12] – i.e. the nuclear charge distribution in the laboratory frame – of states with angular momentum $J \neq 0, \frac{1}{2}$ [11, 12]. In fact, the $E1$ *polarizability* gives rise to extra deformation, which may affect extracted

reduced transition probabilities, i.e. $B(E2)$ values, and shift Q_S values toward more prolate shapes [14]. The determination of the polarizability parameter κ is therefore relevant to the determination of collective properties such as B(E2) and Q_S values [15, 16].

More generally, σ_{-2} values should include both electric (α_{E1}) and magnetic (χ_{M1}) dipole polarizabilities [17],

$$\sigma_{-2} = \frac{2\pi^2}{\hbar c}(\alpha_{E1} + \chi_{M1}). \tag{6}$$

Similarly, χ_{M1} is a measure of the magnetic dipole response, **M**, to a magnetic field, **B**, i.e. $\mathbf{M} = \chi_{M1} \cdot \mathbf{B}$ [18], and can be decomposed into paramagnetic (χ_{M1}^{para}) and diamagnetic (χ_{M1}^{dia}) susceptibilities,

$$\chi_{M1} = \chi_{M1}^{para} + \chi_{M1}^{dia} = 2\sum_n \frac{\langle i \parallel \hat{M}1 \parallel n\rangle\langle n \parallel \hat{M}1 \parallel i\rangle}{E_\gamma} - \frac{Ze^2}{6mc^2}\langle r^2\rangle. \tag{7}$$

Permanent magnetic dipole moments, i.e. paramagnetism, is dominant for $A < 20$ nuclides and may have a substantial contribution to σ_{-2} values (e.g. ^{6}Li and ^{7}Li), whereas diamagnetism has negligible effects [17, 18].

Because of the $1/{E_\gamma}^2$ weighting in Eq. 4, σ_{-2} values are sensitite to low-energy E_γ and not significantly affected by nucleon resonances at high E_γ (e.g. pion exchanges at $E_\gamma \gtrsim 140$ MeV) [19]; hence, they are extremely sensitive measures – unlike σ_{total} – of long-range correlations in the nuclear wave functions.

2 Low energy enhancement of the photon strength function

A potentially larger effect to σ_{-2} values at higher excitation energies in the quasi-continuum region may arise from the low-energy enhancement (LEE) of the radiative or photon strength function $f(E_\gamma)$. The photon strength function $f(E_\gamma)$ characterizes average EM decay and absorption properties of excited nuclei. Recent measurements of $f(E_\gamma)$ by the Oslo group have revealed an enhancement at low E_γ [20–23]. These measurements are performed in the quasi-continuum energy region and assumes the validity of the Brink-Axel hypothesis [24, 25], which states that $f(E_\gamma)$ is independent of the particular structure and only depends on E_γ, i.e. GDR properties are similar for all initial nuclear states. To date, the EM character of the LEE remains undetermined experimentally, although polarization asymmetry measurements of γ rays in ^{56}Fe show a dominant dipole radiation at $E_\gamma < 1.5$ MeV [26]. Various interpretations of the LEE have been proposed, explaining its dipole origin as $M1$ [27–32] and $E1$ [33] dipole radiation [34]. Shell-model (SM) calculations consistently support the $M1$ nature of the LEE [27–30]. The main purpose of this work is to quantify the potentially large contribution from the LEE anomaly to the nuclear polarizability and σ_{-2} values assuming dipole radiation and validity of the Brink-Axel hypothesis.

3 Systematics and results

The LEE is generally observed in medium-mass nuclei in the $A \approx 50$ and 90 mass regions and only for ^{105}Cd, ^{138,139}La and ^{151,153}Sm [35–37] in heavy-mass nuclei. These nuclei, spanning the mass range $A = 45-153$, have been considered in order to obtain a systematic

study of LEE + GDR effects on σ_{-2} values, which requires the combined analysis of LEE and GDR cross sections,

$$\sigma_{total}(E_\gamma) = \sigma_{GDR}(E_\gamma) + \sigma_{LEE}(E_\gamma), \tag{8}$$

where $\sigma_{GDR}(E_\gamma) = \sigma(\gamma, p) + \sigma(\gamma, n) + \sigma(\gamma, 2n) + \sigma(\gamma, np)$ is given by photo-absorption reactions at energies above nucleon threshold, and $\sigma_{LEE}(E_\gamma)$ is the cross section contribution from the LEE region below the neutron threshold. The GDR data are obtained from the experimental nuclear-reaction databases EXFOR https://www-nds.iaea.org/exfor/exfor.htm and ENDF https://www.nndc.bnl.gov/ensdf/, whereas the LEE data come from the Oslo compilation of $f(E_\gamma)$ https://www.mn.uio.no/fysikk/english/research/about/infrastructure/ocl/nuclear-physics-research/compilation/, in units of MeV^{-3}. The LEE data can be converted to cross sections as follows [38],

$$\sigma_{LEE}(E_\gamma) = \pi^2 g_J (\hbar c)^2 f(E_\gamma) E_\gamma \ \ [\mathrm{mb}], \tag{9}$$

where g_J is the statistical factor $g_J = \frac{2J_f+1}{2J_i+1}$ with spins J_i and J_f corresponding to initial and final states, respectively. The magnitude of g_J affects σ_{-2} and polarizability values proportionally. Considering the dipole character of the LEE, $g_J = 1$ is a reasonable approximation for dipole transitions, particularly for $\Delta J = 0$ and $\Delta J = 1$ transitions. A value of $g_J = 3$ is more suitable for even-even nuclei, resulting from $1^- \rightarrow 0^+$ transitions in the GDR.

The combination of GDR and LEE contributions may be arguable, because $\sigma_{GDR}(E_\gamma)$ corresponds to transitions between excited states $|n\rangle$ in the GDR region and the g.s. $|i\rangle$, whereas $\sigma_{LEE}(E_\gamma)$ results from transitions between excited states in the quasi-continuum region. Recent studies of $f(E_\gamma)$ by Guttormsen and co-workers [39] in the LEE region support the validity of the Brink-Axel hypothesis at different excitation energies. This, together with the fact that GDR studies of hot nuclei (at relatively low temperatures T and spin J) and cold nuclei ($T = 0$ for the ground state) present similar features [9, 40], may allow for combining the LEE and GDR cross sections [41].

An interpolation method for calculating $\sigma_{total}(E_\gamma)$ and σ_{-2} values has been used in this work. This method is independent of any physical phenomena and operates by creating a function – cubic or 4^{th} order polynomial – that interpolates between the fixed experimental data points. As an example, Fig. 1 shows the total cross section of ^{56}Fe with a cubic interpolation function (solid blue line). The resulting function is integrated accordingly to obtain $\sigma_{total}(E_\gamma)$, which yields the σ_{-2} values listed in Table 1 and shown in Fig. 2.

Most nuclei present an energy gap (missing experimental data) between the LEE and GDR data, which may include the $M1$ spin-flip resonance and the pygmy dipole resonances (PDR) for neutron-rich nuclei. Therefore, data from ENDF https://www.nndc.bnl.gov/ensdf/ – when available – have been used to fill the gap, as shown in Fig. 3a. Additionally, data near nucleon threshold energies generally present large uncertainties and have been excluded.

Because of minimal RMS errors, a cubic-spline interpolation has been selected as the interpolating function throughout this work. Similar results are obtained using a 4^{th}-order polynomial interpolation. Lower and higher order interpolations present unexpected structures (bumps) in the energy-gap region and above. This is shown in Fig. 3b for the ^{45}Sc data fitted to a quadratic interpolation function. The errors associated to σ_{-2} values are calculated from upper and lower *loci* limits of $\sigma_{total}(E_\gamma)$, including LEE and GDR contributions as shown in Fig. 4, which yields an uncertainty of 7%. Uncertainties for the interpolation data spanning the gap and extrapolated data are treated as three points standard deviation of the mean, in order to determine the upper and lower limits for these data sets. Most of the considered nuclei are stable, except ^{50}V, ^{138}La and ^{153}Sm with no experimental GDR cross

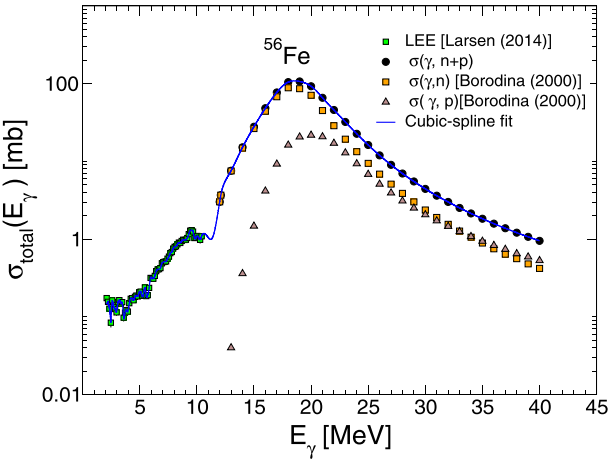

Fig. 1 $\sigma_{total}(E_\gamma)$ vs E_γ on a log scale on the y-axis showing the interpolation function data (solid blue line) for ^{56}Fe, the green squares represent $\sigma_{LEE}(E_\gamma)$ and black filled circles the sum of proton and neutron emission cross sections for the GDR

Table 1 Contributions of GDR and LEE cross-sections to σ_{-2} and κ values

Nucleus	$E_{\gamma(max)}$(GDR) (MeV)	$E_{\gamma(max)}$(LEE) (MeV)	σ_{-2}(total) (μb/MeV)	σ_{-2}(LEE) (μb/MeV)	**C** (%)	κ (with LEE)	[Refs.]
$^{45}_{21}$Sc*	28.1	3.2	1840(130)	178	9.7%	1.35(9)	[42–44]
$^{50}_{23}$V	27.8	3.1	1458(100)	43	2.9%	0.89(5)	[45, 46]
$^{51}_{23}$V	27.8	3.1	1472(100)	49	3.3%	0.87(5)	[45, 46]
$^{56}_{26}$Fe*	40.0	3.8	2231(155)	141	6.3%	1.13(6)	[47, 48]
$^{76}_{32}$Ge	26.5	2.3	3189(225)	86	2.7%	0.97(5)	[49, 50]
$^{92}_{40}$Zr	27.8	2.2	3131(220)	34	1.1%	0.70(3)	[51–53]
$^{95}_{42}$Mo	27.8	2.5	4743(330)	81	1.7%	1.00(5)	[54, 55]
$^{138}_{57}$La	24.3	1.9	7983(560)	319	0.4%	0.90(5)	[36, 56]
$^{139}_{57}$La	24.3	2.5	8015(560)	561	0.7%	0.90(4)	[36, 56]
$^{153}_{62}$Sm	20.0	1.6	9999(700)	267	2.7%	0.95(5)	[37, 57]

Data have been extracted from EXFOR https://www-nds.iaea.org/exfor/exfor.htm, ENDF https://www.nndc.bnl.gov/ensdf/ and the Oslo compilation http://www.mn.uio.no/fysikk/english/research/\about/infrastructure/OCL/nuclear-physics-research/compilation/. An asterisk indicates that the σ_{-2} value includes $\sigma(\gamma, p)$ contributions. **C** is a measure of the LEE contribution to total σ_{-2} values. This table is adapted from Ref. [41]

sections. Therefore, GDR data of stable neighboring isotopes were used, i.e. ^{51}V, ^{139}La and ^{152}Sm, under the assumption that neighboring nuclei present similar $f(E_\gamma)$ [22] and the fact that σ_{-2} values show a strong dependence on nuclear mass A.

Setting up the low-energy cut-off, $E_{\gamma_{min}}$, for the LEE is not obvious. In our previous study, we extrapolated the LEE data down to 800 keV from experimental observations which show $E_{\gamma_{min}} \approx 1$ MeV for most nuclei, except for ^{153}Sm where measurements were carried out down to $E_{\gamma_{min}} = 645$ keV. The σ_{-2}(LEE) values in Table 1 are calculated between the

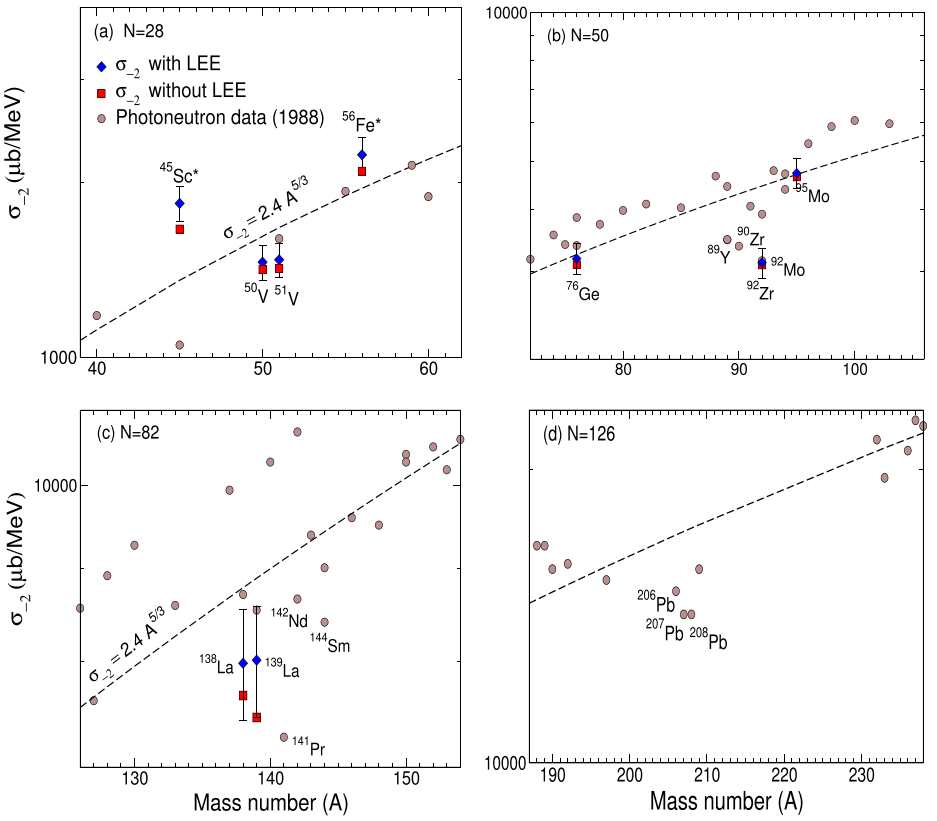

Fig. 2 σ_{-2} *vs* A on a log scale on the y-axis for nuclei around **a** $N = 28$, **b** $N = 50$, **c** $N = 82$ and **d** $N = 126$. Data are from the photo-neutron cross-section evaluation (solid circles) [6] and σ_{-2} values listed in Table 1, excluding (squares) and including (diamonds) the LEE contributions. For comparison, Eq. 5 (dashed line) is plotted

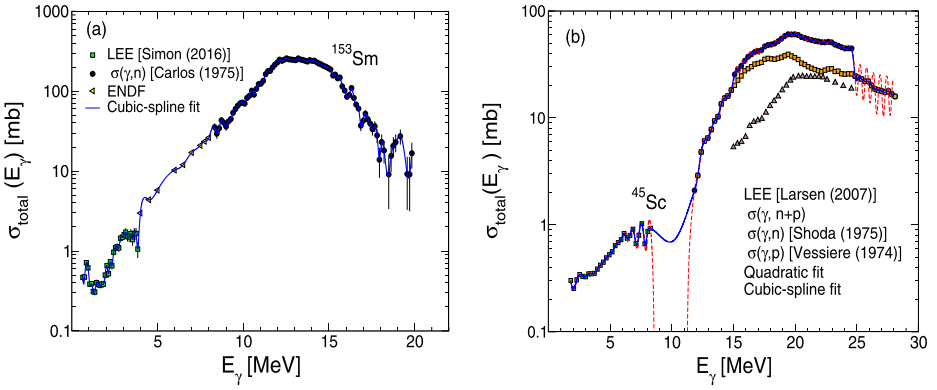

Fig. 3 $\sigma_{total}(E_\gamma)$ vs E_γ in log scale on the y-axis for **a** ^{153}Sm from ENDF data (triangles) and **b** ^{45}Sc interpolated with a cubic (solid blue line) and quadratic (red dashed line) functions

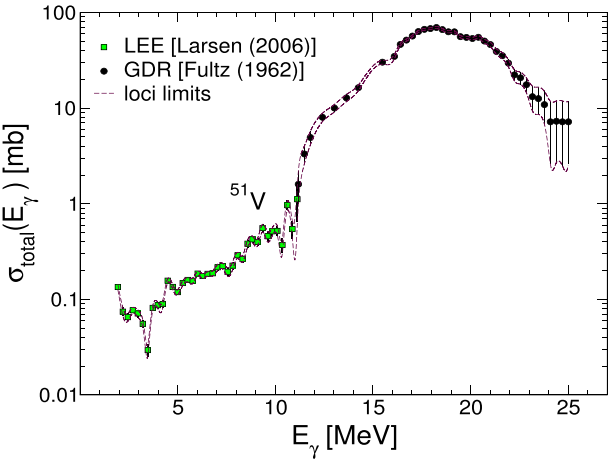

Fig. 4 $\sigma_{total}(E_\gamma)$ vs E_γ in log scale on the y-axis for ^{51}V showing the upper and lower loci limits used to estimate the error

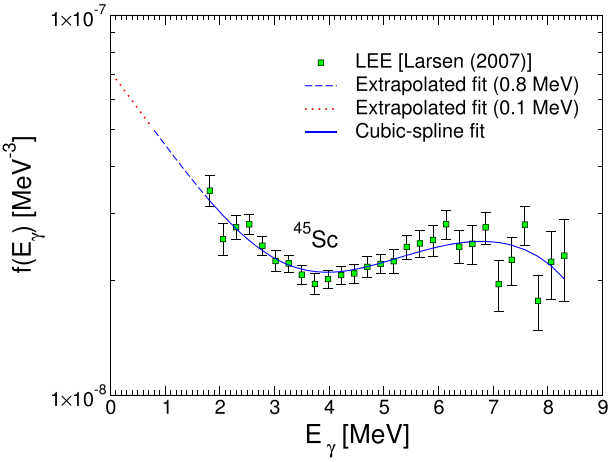

Fig. 5 $f(E_\gamma)$ for ^{45}Sc fitted with a cubic polynomial (solid blue line), including extrapolated data to $E_{\gamma_{min}} = 0.8$ MeV (dashed blue line) and $E_{\gamma_{min}} = 0.1$ MeV (red dotted line)

lower $E_{\gamma_{min}} = 0.8$ MeV and $E_{\gamma_{max}}$(LEE), where the LEE starts [41]. Recent SM studies [26, 29, 31] explore, however, the behavior of $f(E_\gamma)$ at very low E_γ, supporting the continuation of the LEE down to $E_{\gamma_{min}} = 0$. Consequently, we have investigated this situation and Fig. 5 shows an extrapolated fit of $f(E_\gamma)$ to ^{45}Sc data down to $E_{\gamma_{min}} = 0.1$ MeV. Similar fits were done for ^{51}V and ^{56}Fe to explore $f(E_\gamma)$ in the $A \approx 50$ region and the results are listed in Table 2. A large enhancement of σ_{-2} values is found for ^{45}Sc and ^{56}Fe as compared with ^{51}V. If these predictions of $f(E_\gamma)$ for $E_{\gamma_{min}} \rightarrow 0$ MeV are consistent with experimental findings, reaction rates in nucleosynthesis following rapid-neutron capture – the r-process – may strongly be affected together with the predicted abundances of nuclei [36, 58–60].

Table 2 Contributions of the LEE with $E_{\gamma_{min}} = 0.1$ MeV represented by **C**

Nucleus	$E_{\gamma(min)}$ (MeV)	$E_{\gamma(max)}$(GDR) (MeV)	$E_{\gamma(max)}$(LEE) (MeV)	σ_{-2}(total) (μb/MeV)	σ_{-2}(LEE) (μb/MeV)	**C** %
$^{45}_{21}$Sc	0.1	28	3.2	2488	873	35.1 %
$^{51}_{23}$V	0.1	27.8	3.1	1564	140	9 %
$^{56}_{26}$Fe	0.1	40	3.8	2658	568	21.4 %

$E_{\gamma(max)}$(LEE) is the energy at which the LEE starts

4 Discussion and conclusion

As shown in our previous work [41], drops of nuclear polarizability are evident in nuclei with or near magic numbers $N = 28$, 50, 82 and 126, which are characterized by values of $\kappa < 1$. The work presented here expands on the data analysis presented in Ref. [41], but also provides an additional piece of evidence for shell effects. As illustrated when comparing Tables 1 and 2 for the neighboring ^{45}Sc, ^{51}V and ^{56}Fe nuclei, it is clear that once we extrapolate the LEE down to $E_\gamma = 100$ keV (see Table 2), σ_{-2} values show a higher sensitivity to shell effects. That is, while the LEE contribution for the semi-magic nucleus ^{51}V slightly increases, there is relatively a much larger enhancement of σ_{-2} values for ^{45}Sc and ^{56}Fe.

Conclusively, σ_{-2} values can be assigned as a new spectroscopic probe to extract information on shell effects at high-excitation energies; in the same way as atomic masses are useful to study nuclear structure via nuclear binding energies. Finally, the observed deviations from the actual GDR effects may support the validity of 1) recent large-scale SM calculations, which predict the $M1$ nature of the LEE, and 2) the generalized Brink-Axel hypothesis, which surprisingly, also allows for structural changes. This work emphasizes the need for new photo-absorption cross-section and $f(E_\gamma)$ measurements, and opens a new research avenue to investigate the existence and evolution of magic numbers at high-excitation energies from σ_{-2} values [41].

Acknowledgements This work was supported by the National Research Foundation of South Africa under Grant 93500, the MaNus/MatSci program and the SA-CERN collaboration.

References

1. Migdal, A.: Quadrupole and dipole gamma-radiation of nuclei. J. Exptl. Theoret. Phys. U.S.S.R. **15**, 81 (1945)
2. Steinwedel, H., Jensen, J.H.D., Jensen, P.: Nuclear dipole vibrations. Phys. Rev. **79**, 1019 (1950)
3. Bethe, H.A., Bacher, R.F.: Stationary states of nuclei. Rev. Mod. Phys. **8**, 82 (1936)
4. von Weizsäcker, C.F.: Zur Theorie der Kernmassen. Z. Phys. **96**, 431 (1935)
5. Migdal, A.B., Lushnikov, A.A., Zaretsky, D.F.: Theory of dipole photoabsorption of nuclei. Nucl. Phys. A **66**, 193 (1965)

6. Dietrich, S.S., Berman, B.L.: Atlas of photoneutron cross sections obtained with monoenergetic photons. At. Data Nucl. Data Tables **38**, 199 (1988)
7. Orce, J.N.: New formulas for the (-2) moment of the photoabsorption cross section, σ_{-2}, Phys. Rev. C **91**, 064602 (2015)
8. Levinger, J.S.: Migdal's and Khokhlov's calculations of the nuclear photoeffect. Phys. Rev. **107**, 554 (1957)
9. Gaardhøje, J.J.: Nuclear structure at high excitation energy studied with giant resonances. Annu. Rev. Nucl. Part. Sci. **42**, 483 (1992)
10. Eichler, J.: Second-order coulomb excitation via the giant dipole resonance. Phys. Rev. **133**, B1162 (1964)
11. de Boer, J., Eichler, J.: The reorientation effect. Adv. Nucl. Phys. **1**, 1 (1968)
12. Häusser, O.: Nuclear Spectroscopy and Reactions C, edited by J. Cerny. Academic, New York (1974)
13. Alder, K., Winther, A.: Electromagnetic Excitation. North-Holland, Amsterdam (1975)
14. Häusser, O. et al.: E1 polarization in coulomb excitation of ^{7}Li. Nucl. Phys. A **212**, 613 (1973)
15. Orce, J.N., et al.: Reorientation-effect measurement of the $\langle 2_1^+ \parallel \mathrm{E2} \parallel 2_1^+ \rangle$ matrix element in ^{10}Be. Phys. Rev. C **86**, 041303(R) (2012)
16. Raju, M.K. et al.: Reorientation-effect measurement of the first 2^+ state in ^{12}C: confirmation of oblate deformation. Phys. Lett. B. **777**, 250 (2018)
17. Knüpfer, W., Richter, A.: Effect of the nuclear magnetic susceptibility on the evaluation of the electric dipole polarizability. Phys. Lett. B **107**, 325 (1981)
18. Knüpfer, W., Richter, A.: On the scaling of the paramagnetic susceptibility of atoms, nuclei and nucleons. Z. Phys. A **320**, 253 (1985)
19. Ahrens, J., Gimm, H., Zieger, A., Ziegler, B.: Experimental values for the static nuclear polarizability. Il Nuovo Cimento A **32**(3), 364 (1976)
20. Voinov, A., et al.: Large enhancement of radiative strength for soft transitions in the quasicontinuum. Phys. Rev. Lett. **93**, 142504 (2004)
21. Schiller, A. et al.: Extraction of level density and γ strength function from primary γ spectra. Nucl. Instr. Meth. Phys. Res. A **447**, 498 (2000)
22. Guttormsen, M., et al.: Radiative strength functions in $^{93-98}$Mo. Phys. Rev. C **71**, 044307 (2005)
23. Wiedeking, M., et al.: Low-energy enhancement in the photon strength of ^{95}Mo. Phys. Rev. Lett. **108**, 162503 (2012)
24. Brink, D.: Doctoral Thesis. Oxford University (1955)
25. Axel, P.: Electric dipole ground-state transition width strength function and 7-MeV photon interactions. Phys. Rev. **126**, 671 (1962)
26. Jones, M.D., et al.: Examination of the low-energy enhancement of the γ-ray strength function of ^{56}Fe. Phys. Rev. C **97**, 024327 (2018)
27. Schwengner, R., Frauendorf, S., Larsen, A.C.: Low-energy enhancement of magnetic dipole radiation. Phys. Rev. Lett. **111**, 232504 (2013)
28. Brown, B.A., Larsen, A.C.: Large Low-Energy M1 Strength for ^{56,57}Fe within the Nuclear Shell Model. Phys. Rev. Lett. **113**, 252502 (2014)
29. Sieja, K.: Electric and magnetic dipole strength at low energy. Phys. Rev. Lett. **119**, 052502 (2017)
30. Sieja, K.: Low energy dipole strength from large scale shell model calculations. EPJ Web of Conferences **146**, 05004 (2017)
31. Midtbo, J.E., et al.: Consolidating the concept of low-energy magnetic dipole decay radiation. Phys. Rev. C **98**, 064321 (2018)
32. Larsen, A.C., et al.: Enhanced low-energy γ-decay strength of ^{70}Ni and its robustness within the shell model. Phys. Rev. C **97**, 054329 (2018)
33. Litvinova, E., Belov, N.: Low-energy limit of the radiative dipole strength in nuclei. Phys. Rev. C **88**, 031302(R) (2013)
34. Jackson, J.D.: Classical Electrodynamics. Wiley, Hoboken (1962)
35. Larsen, A.C., et al.: Transitional γ strength in Cd isotopes. Phys. Rev. C **87**, 014319 (2013)
36. Kheswa, B.V. et al.: Galactic production of ^{138}La: Impact of ^{138,139}La statistical properties. Phys. Lett. B **744**, 268 (2015)
37. Simon, A., et al.: First observation of low-energy γ-ray enhancement in the rare-earth region. Phys. Rev. C **93**, 034303 (2016)
38. Bartholomew, G.A., Earle, E.D., Ferguson, A.J., Knowles, J.W., Lone, M.A.: Gamma-ray strength functions. Adv. Nucl. Phys. **7**, 229 (2012)
39. Guttormsen, M., et al.: Validity of the generalised Brink-Axel hypothesis. Phys. Rev. Lett. **116**, 012502 (2016)

40. Schiller, A., Thoennessen, M.: Compilation of electric dipole resonances built on excited states. Atom. Data Nucl. Data Tables **93**, 549 (2007)
41. Ngwetsheni, C., Orce, J.N.: Continuing influence of shell effects at high-excitation energies. Phys. Lett. B **792**, 335 (2019)
42. Vessiere, A. et al.: A study of the photoneutron contribution to the giant dipole resonance of sd shell nuclei. Nucl. Phys. A **227**, 513 (1974)
43. Larsen, A.C., et al.: Nuclear level densities and γ-ray strength functions in ^{44,45}Sc. Phys. Rev. C **76**, 044303 (2007)
44. Shoda, K.: (γ,p) cross sections and isospin splitting of the giant dipole resonance in N = 50 nuclei. Nucl. Phys. A **239**, 397 (1975)
45. Fultz, S.C. et al.: Photoneutron cross sections for ^{51}V and ^{59}Co. Phys. Rev **128**, 2345 (1962)
46. Larsen, A.C., et al.: Microcanonical entropies and radiative strength functions of ^{50,51}V. Phys. Rev. C **73**, 064301 (2006)
47. Borodina, S.S. et al.: ^{54,56}Fe and ^{58,60}Ni(γ,n), (γ,p), (γ,np), and (γ,2n) reaction cross sections evaluation using the model of the GDR state decay channel competition phenomenological description. Moscow State Univ. Inst. of Nucl. Phys. Rep., 6 (2000)
48. Larsen A.C., et al.: Evidence for the dipole nature of the low-energy γ Enhancement in ^{56}Fe. Phys. Rev. Lett. **111**, 242504 (2013)
49. Carlos, P. et al.: A study of the photoneutron contribution to the giant dipole resonance of nuclei in the 64 ≦ A ≦ 86 m ass region. Nucl. Phys. A **258**, 365 (1976)
50. Spyrou, A., et al.: Novel technique for constraining r-process (n,γ) reaction rates. Phys. Rev. Lett. **113**, 232502 (2014)
51. Berman, B.L. et al.: Photoneutron cross sections for ^{90}Zr, ^{91}Zr, ^{92}Zr, ^{94}Zr and ^{89}Y. Phys. Rev. **162**, 1098 (1967)
52. Guttormsen, M., et al.: Quasicontinuum γ decay of ^{91,92}Zr: benchmarking indirect (n,γ) cross section measurements for the s process. Phys. Rev. C **96**, 024313 (2017)
53. Utsunomiya, H., et al.: M1 γ-strength for zirconium nuclei in the photoneutron channel. Phys. Rev. Lett. **100**, 162502 (2008)
54. Beil, H. et al.: A study of the photoneutron contribution to the giant dipole resonance in doubly even Mo isotopes. Nucl. Phys. A **227**, 427 (1974)
55. Utsunomiya, H., et al.: Photoneutron cross sections for Mo isotopes: a step toward a unified understanding of (γ, n) and (n, γ) reactions. Phys. Rev. C **88**, 015805 (2013)
56. Beil, H. et al.: Giant dipole resonance in N = 82 nuclei. Nucl. Phys. A **172**, 426 (1971)
57. Carlos, P. et al.: The giant dipole resonance in the transition region of the samarium isotopes. Nucl. Phys. A **225**, 171 (1974)
58. Arnould, M., Goriely, S., Takahashi, K.: The r-process of stellar nucleosynthesis: astrophysics and nuclear physics achievements and mysteries. Phys. Rep. **450**, 97 (2007)
59. Larsen, A.C., Goriely, S.: Impact of a low-energy enhancement in the γ-ray strength function on the neutron-capture cross section. Phys. Rev. C **82**, 014318 (2010)
60. Larsen, A.C., Spyrou, A., Liddick, S.N., Guttormsen, M.: Novel techniques for constraining neutron-capture rates relevant for *r*-Process heavy-element nucleosynthesis. Prog. Part. Nucl. Phys **107**, 69 (2019)

Terms and Conditions

Springer Nature journal content, brought to you courtesy of Springer Nature Customer Service Center GmbH ("Springer Nature").

Springer Nature supports a reasonable amount of sharing of research papers by authors, subscribers and authorised users ("Users"), for small-scale personal, non-commercial use provided that all copyright, trade and service marks and other proprietary notices are maintained. By accessing, sharing, receiving or otherwise using the Springer Nature journal content you agree to these terms of use ("Terms"). For these purposes, Springer Nature considers academic use (by researchers and students) to be non-commercial.

These Terms are supplementary and will apply in addition to any applicable website terms and conditions, a relevant site licence or a personal subscription. These Terms will prevail over any conflict or ambiguity with regards to the relevant terms, a site licence or a personal subscription (to the extent of the conflict or ambiguity only). For Creative Commons-licensed articles, the terms of the Creative Commons license used will apply.

We collect and use personal data to provide access to the Springer Nature journal content. We may also use these personal data internally within ResearchGate and Springer Nature and as agreed share it, in an anonymised way, for purposes of tracking, analysis and reporting. We will not otherwise disclose your personal data outside the ResearchGate or the Springer Nature group of companies unless we have your permission as detailed in the Privacy Policy.

While Users may use the Springer Nature journal content for small scale, personal non-commercial use, it is important to note that Users may not:

1. use such content for the purpose of providing other users with access on a regular or large scale basis or as a means to circumvent access control;
2. use such content where to do so would be considered a criminal or statutory offence in any jurisdiction, or gives rise to civil liability, or is otherwise unlawful;
3. falsely or misleadingly imply or suggest endorsement, approval , sponsorship, or association unless explicitly agreed to by Springer Nature in writing;
4. use bots or other automated methods to access the content or redirect messages
5. override any security feature or exclusionary protocol; or
6. share the content in order to create substitute for Springer Nature products or services or a systematic database of Springer Nature journal content.

In line with the restriction against commercial use, Springer Nature does not permit the creation of a product or service that creates revenue, royalties, rent or income from our content or its inclusion as part of a paid for service or for other commercial gain. Springer Nature journal content cannot be used for inter-library loans and librarians may not upload Springer Nature journal content on a large scale into their, or any other, institutional repository.

These terms of use are reviewed regularly and may be amended at any time. Springer Nature is not obligated to publish any information or content on this website and may remove it or features or functionality at our sole discretion, at any time with or without notice. Springer Nature may revoke this licence to you at any time and remove access to any copies of the Springer Nature journal content which have been saved.

To the fullest extent permitted by law, Springer Nature makes no warranties, representations or guarantees to Users, either express or implied with respect to the Springer nature journal content and all parties disclaim and waive any implied warranties or warranties imposed by law, including merchantability or fitness for any particular purpose.

Please note that these rights do not automatically extend to content, data or other material published by Springer Nature that may be licensed from third parties.

If you would like to use or distribute our Springer Nature journal content to a wider audience or on a regular basis or in any other manner not expressly permitted by these Terms, please contact Springer Nature at

onlineservice@springernature.com